

THE DIURNAL CYCLE AND EVENT-SCALE PRECIPITATION CHARACTERISTICS IN GALÁPAGOS AT DIFFERENT ALTITUDES DURING ENSO 2022-2024

PABLO TENELANDA, NAZLI TURINI, JOHANNA ORELLANA-ALVEAR, BYRON DELGADO MALDONADO, JÖRG BENDIX and ROLANDO CÉLLERI

With 17 figures and 20 tables

Received 7 October 2024 · Accepted 13 April 2025

Summary: An understanding of sub-hourly precipitation variability in the Galapagos Islands is crucial for water resource management and effective biodiversity conservation. This study compares the diurnal cycle and event-scale precipitation characteristics (ESPC), such as mean and maximum intensity, duration and rainfall accumulation at different altitudes during El Niño-Southern Oscillation (ENSO) 2022-2024 on Santa Cruz Island. The La Niña phase was analyzed from April 2022 to January 2023 and the El Niño phase from June 2023 to April 2024. Precipitation data, recorded every 10 minutes, was collected from a recently established network of automatic weather stations, which were strategically positioned at three windward and two leeward sites. The results suggest that the diurnal cycle was influenced by altitude, with a maximum variability between morning and afternoon, regardless of ENSO phase. During La Niña, ESPC exhibited similarities at intermediate altitudes at both windward and leeward sides. However, rainfall events at the island's summit were less intense and of longer duration. During El Niño, the highest intensities were observed along the coast and at intermediate altitudes of both windward and leeward locations. In contrast, at the top of the island, rainfall events were less intense and more prolonged. At all altitudes, more than half of the rainfall events corresponded to garúa events, and at the top of the island, almost all events were of this type. At this altitude, the contribution of garúa events to the total rainfall accumulation was 80% and 85% for La Niña and El Niño, respectively. This study provides a detailed analysis of how sub-hourly precipitation varies significantly at different altitudes on the windward and leeward sides as a function of ENSO phases, providing valuable baseline information for future studies in this unique and fragile ecosystem.

Keywords: Galápagos, Santa Cruz Island, El Niño, La Niña, diurnal cycle, event-scale precipitation characteristics, windward, leeward

1 Introduction

The El Niño Southern Oscillation (ENSO) is an ocean-atmosphere phenomenon that has a major impact on global interannual climate variability, with important effects on biodiversity and water resource management (JONAITIS et al. 2021, RHOADES et al. 2024). ENSO consists of two phases: La Niña and El Niño, which are associated with negative and positive sea surface temperature (SST) anomalies in the equatorial Pacific Ocean, respectively (HARTMANN 2016). These phases usually occur at intervals of 2 to 7 years. During El Niño, SSTs are warmer than average in the central and eastern Pacific, while they are cooler in the western Pacific and in the north-central and south-central areas. In contrast, during La Niña, opposite anomalies are observed, with cooler SSTs in the eastern Pacific and warmer SSTs in the western Pacific (WANG et al. 2017). Variations in SST alter the moisture content of the air transported by the trade winds, significantly influencing global precipitation variability. During El Niño, precipitation frequency

in the western tropical Pacific may be reduced due to large-scale weakening of the trade winds and atmospheric convergence (LI et al. 2020). In Singapore, seasonal rainfall totals are highest during La Niña, with twice as many rainfall hours as during El Niño (LI et al. 2016). In Malaysia, both dry and wet precipitation extremes are influenced by El Niño and La Niña, respectively, depending on location and season (TANGANG et al. 2017). In the Hawaiian Islands, ENSO effects are consistent across the islands, where El Niño phase results in below-average precipitation, while La Niña does not always result in above-average precipitation (KOLIVRAS & COMRIE 2007). In the study by BENDIX & BENDIX (2006), it was observed that during El Niño 1991-92, heavy rainfall, especially along the coast of Ecuador and northern Peru, was due to intense SST gradients that generate moist atmospheric instability. However, the total amount of precipitation recorded along the coast of Ecuador was greater than that observed in the western Pacific (north and south of the Galapagos Archipelago), because the formation and dynamics of heavy pre-

precipitation in Ecuador and northern Peru during the 1991-92 El Niño were influenced by a diurnal land-sea wind system, sometimes coupled with thermally driven upwelling winds (BENDIX 2000).

The Galapagos Archipelago, known for its endemic species and great biodiversity, experiences two seasons during the year due to the movement of the Intertropical Convergence Zone (ITCZ). The cool dry season lasts from June to December, while the warm wet season lasts from January to May (TRUEMAN & D'OZOUVILLE 2010). It is also known that the highlands above 250 m asl are wetter than the lowlands (SACHS & LADD 2010). This temporal and altitudinal behavior of precipitation is similar to that observed on other tropical islands (MAIR & FARES 2011, RÉCHOU et al. 2019, SANCHEZ-MORENO et al. 2014, SMITH et al. 2009, TANTELINIAINA et al. 2020). However, interannual precipitation variability is influenced by the ENSO phenomenon, which occurs in its two phases, El Niño and La Niña (DUEÑAS et al. 2021). During El Niño, there is an increase in convective clouds and heavy rainfall, as well as a period of extension of the warm season into the cool season months (CONROY et al. 2008). Conversely, during La Niña, the region experiences drought conditions. (SNELL & REA 1999, WINGFIELD et al. 2018). PALTÁN et al. (2021) studied changes in meteorological variables on Santa Cruz Island since 1980 over a 30-year period, using data from both lowland and highland sites (at 194 m asl). Their study found that the warm season is responsible for 75% and 55% of the annual precipitation in the lowlands and highlands, respectively. Furthermore, they observed that precipitation is highly variable, especially during the warm season, due to the influence of ENSO years (1982-83 and 1997-98), in which precipitation was almost three times higher than in non-El Niño years. The 1982-83 El Niño has been the most severe in terms of precipitation compared to previous El Niño phases since the one recorded in 1952 (GRANT 1984). However, total precipitation was similar between El Niño 1982-83 and 1997-98, although they differed in medium-term precipitation intensity. In contrast, some phases, such as El Niño 1975-76 and 1992-93, recorded higher precipitation during the warm season, from January to April (SNELL & REA 1999). In addition, the frequency and intensity of El Niño phases have increased from moderate to strong over the past 3500 years (ZHANG et al. 2014), and these are likely to become more intense in the future (SACHS & LADD 2010). Through monthly and daily isotopic analysis conducted on Santa Cruz Island by (MARTIN et al. 2018), on a north-south transect with an altitu-

dinal range of 613 m asl, it was observed that most rainfall events in the lowlands were drizzle ('garúa') or light rain, with precipitation rates below 1 mm/day or between 1 and 10 mm/day, respectively. This pattern was also observed in the highlands. During El Niño 1997-98, abundant rainfall occurred with low $\delta^{18}O_p$ values of precipitation. Furthermore, from La Niña to El Niño, most of the isotopically observed rainfall events were drizzle or garúa of local origin with high $\delta^{18}O_p$ values of precipitation. The effects of these phenomena have important implications for biodiversity and water supply from rainfall dependent sources (DOMÍNGUEZ et al. 2016, PRYET et al. 2012), as observed during El Niño 1982-83 and 1997-98, which had significant impacts on Galapagos ecosystems and biodiversity (VARGAS et al. 2006). All these studies were based on low temporal resolution data, such as monthly and daily records. Due to this limitation, there is a knowledge gap in the analysis of precipitation using high-resolution temporal data.

Analysis of precipitation using high-resolution temporal data provides more detailed and accurate information on its characteristics and variability, allowing a deeper understanding that could not be achieved with daily and monthly data. Intensity and duration of a rainfall event are important characteristics that provide key information for understanding hydrological processes and their impacts such as flooding, soil erosion, landslides, etc. (CHEN et al. 2015, MINEA et al. 2016). Extreme events of high intensity and short duration are of great importance as they can trigger floods and cause significant damage to public infrastructure, agriculture and tourism in tropical islands (CHU et al. 2009, PRIAMBODO et al. 2019, SHARMA et al. 2021). Furthermore, these events are associated with soil erosion, which can result in significant annual soil loss and affect land quality (FIENER et al. 2019). In the agricultural sector, regions with a higher frequency of small-scale rainfall events have shown lower water use efficiency, which presents a challenge to agricultural productivity (SADRAS 2003). Analyzing the diurnal variability of precipitation, it is possible to identify the specific times at which precipitation peaks and troughs occur, allowing a better understanding of the physical mechanisms underlying the formation of precipitation and its relationship to the local climate (BALDYSZ et al. 2024, WU et al. 2008, ZHU et al. 2017).

In this context, the objective of this study is to compare the diurnal cycle and event-scale precipitation characteristics (e.g. intensity, duration, rainfall accumulation) at different altitudes during ENSO 2022-2024 on Santa Cruz Island using sub-hourly

data. This will allow a better understanding of precipitation and will serve as a basis for future studies on water resource management and biodiversity conservation.

2 Materials and methods

2.1 Study area

The study area is the Santa Cruz Island, one of the main islands of the Galápagos archipelago, located approximately 1000 km off the coast of Ecuador (Fig. 1). It is also the most populated island, with an area of 985 km² and a maximum elevation of 864 m asl. Two seasons can be distinguished throughout the year. The cool dry season is from June to December, while the warm wet season is from January to May (TRUEMAN & D'OZOUVILLE 2010). During the warm season, precipitation is variable and convective. On the other hand, during the cool season, cold air ascending the windward slopes condenses from 250 m asl until it reaches the trade wind inversion layer (SACHS & LADD 2010). This layer is formed when the cold air mass is trapped under a warmer air mass and is generally located at about 900 m asl (ZANDER et al. 2023). This meteorological condition results in very fine and low-intensity rain, called drizzle or 'garúa', which causes the highlands to be wetter than the lowlands (GRANT & BOAG 1980, HAMANN 1979). From 1981 to 2017, the mean annual precipitation in the highlands was 1360 mm, contrasting with 500mm in

the lowlands (PALTÁN et al. 2021). However, interannual variations in rainfall are strongly influenced by the two ENSO phases. In the lowlands, the total annual precipitation recorded during the 1998 El Niño was 1687 mm, while the 1999 La Niña resulted in 143 mm (WINGFIELD et al. 2018).

2.2 Data availability

Five Automatic Weather Stations (AWS) were installed on Santa Cruz Island by the DARWIN project "Dynamics of Precipitation in Transition: The water source for the Galápagos Archipelago under climate change". The sites were chosen as to cover different altitudes (lowlands and highland) as well as the windward and leeward sides (Fig. 1). Three stations were located in the southern part of the island, which correspond to the windward side, at 2, 422, and 849 m asl, while two stations were located at 22 and 619 m asl on the leeward side (Tab. 1). Each AWS is equipped with a Lufft WS100 radar precipitation sensor, which records precipitation every 10 minutes with a resolution of 0.01 mm. This sensor uses 24 Hz Doppler radar to calculate precipitation amount and type based on the correlation between droplet velocity and droplet size.

Data collection started between March and April 2022. This data was downloaded and processed by the DARWIN project. A quality control process was then performed on this database to identify missing data, data not available (NA) and erroneous sensor

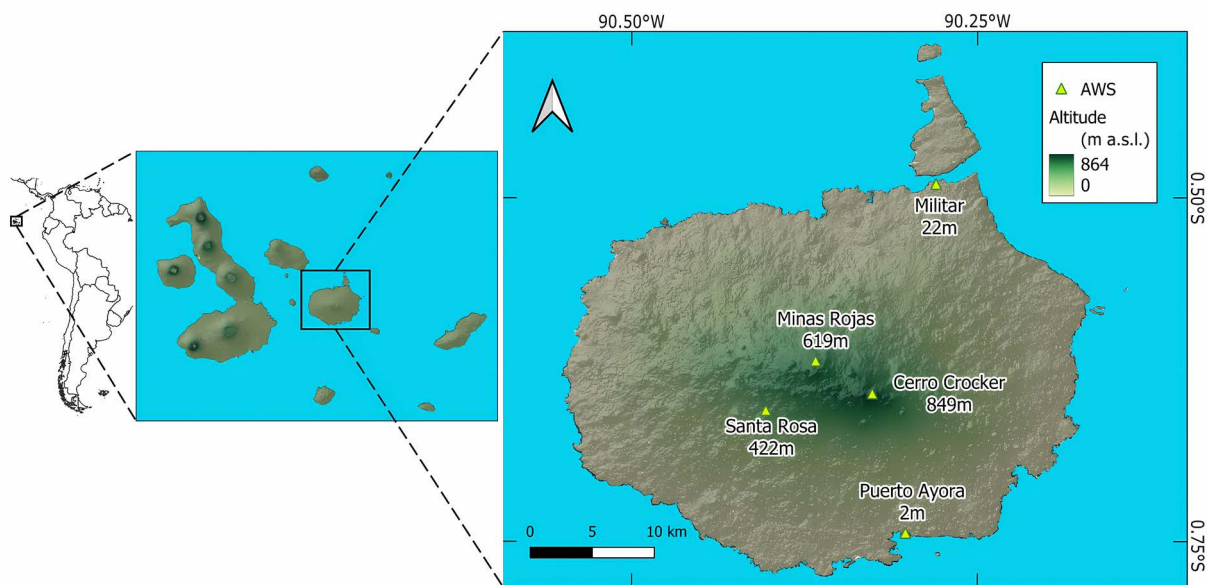


Fig. 1: Geographical map of the study area in Galápagos archipelago

Tab. 1: Name and location of AWS from south to north, as well as on the windward and leeward side. The AWS above 250 belongs to the highlands and AWS below 250 belongs to the lowlands.

AWS name	Alt (m asl)	Site	Latitude (°S)	Longitude (°W)
Puerto Ayora	2	Windward	0.743708	90.3027
Santa Rosa	422	Windward	0.654530	90.4035
Cerro Crocker	849	Windward	0.642398	90.3260
Minas Rojas	619	Leeward	0.618625	90.3673
Militar	22	Leeward	0.489962	90.2808

readings. These values, which generally correspond to sensor failures or anomalous behavior, were identified using statistical tools and detailed visual inspection of the rainfall series over the study period. Erroneous readings with values below the sensor resolution (e.g. 0.00001667 mm) were assigned a value of 0 mm. On the other hand, NA values were removed from the database and, like the missing data, could not be imputed due to the high climatic variability of Galapagos. The percentage of missing data was low, with a maximum of 17% at 22 m asl on the leeward side (Appendix Tab. 4).

The study period was determined based on the Oceanic Niño Index (ONI), whose data are published by the National Oceanic and Atmospheric Administration (NOAA). According to the ONI, La Niña phenomenon is considered to occur when the three-month moving average of sea surface temperature (SST) anomalies in the Niño 3.4 region is less than -0.5°C , while an El Niño occurs when it is greater than 0.5°C (data source <http://www.cpc.ncep.noaa.gov/data/indices/oni.ascii.txt>, last access: 10 September 2024). Therefore, the study period for La Niña was set from April 2022 to January 2023, while El Niño was set from June 2023 to April 2024 (Appendix Fig. 9).

2.3 Selection of rainfall events

In hydrology, there is no clear methodology for selecting rainfall events (DUNKERLEY 2008); however, most studies employ the minimum inter-event time (MIT) to separate rainfall events from continuous rainfall data (BRASIL et al. 2022, CHIN et al. 2016, GAÁL et al. 2014, JOO et al. 2013, NOJUMUDDIN et al. 2018). The MIT represents the minimum time without precipitation that separates one rainfall event from another. However, this parameter may vary depending on the specific study objectives and local site climatic conditions (CARBONE et al. 2014, PADRÓN et al. 2015, TU et al. 2023, WANG et al. 2019). In some cases, the definition of events is complemented by

other parameters, such as the duration and the minimum rainfall accumulation that an event must have (ORELLANA-ALVEAR et al. 2017, SOTTILE et al. 2022, URGILÉS et al. 2021), to eliminate the bias caused by extremely light rainfall events. Therefore, to obtain representative data for each ENSO phase, individual rainfall events at each altitude were identified using three criteria: MIT, minimum rainfall accumulation, and duration. First, the MIT was determined by a sensitivity analysis, varying the time between events until no significant change in the number of events was observed (NIX 1994). Second, the minimum rainfall accumulation was determined by a sensitivity analysis applied to the previously selected events with a specific MIT. This analysis was complemented by a graphical inspection of the distribution of events according to their duration and rainfall accumulation, carried out after the initial selection (Appendix Fig. 12 to 17). Finally, to consider intense events of short duration, a minimum duration equivalent to the 10-minute data recording interval was set.

From the total set of rainfall events identified according to these three criteria, a specific subset corresponding to drizzle or garúa events was extracted. In this study, drizzle events are defined as those with an intensity of 1 mm/h or less (LINSLEY et al. 1975). This subset was selected because of the hydrological and ecological importance of garúa in the Galapagos highlands, especially during the cold and dry season (TRUEMAN & D'OZOUVILLE 2010).

2.4 Altitudinal differences of event-scale precipitation characteristics

The event-scale precipitation characteristics (ESPC) used for the altitudinal comparison were: maximum intensity in ten minutes, mean intensity, duration and rainfall accumulation of the event. In this section, La Niña (from April 2022 to January 2023) and El Niño phases (from June 2023 to April 2024) were analyzed separately, in order to separate

the influence of these phenomena on the altitudinal comparison of the ESPC. First, all rainfall events were compared, and then only garúa events. For the analysis, descriptive statistics using box plots were used to describe the similarities and differences of each ESPC between the different altitudes. Furthermore, the Mann-Whitney U test was used to determine whether these differences were significant. The Mann-Whitney U test, also known as the Wilcoxon rank sum test, is a nonparametric statistical test used to compare the equality of population medians of two independent samples or to test whether they are from the same distribution (WILCOXON 1992). The null hypothesis (H_0) states that there are no significant differences, while the alternative hypothesis (H_1) states that there are significant differences. The p-value is used to decide whether to fail to reject or reject H_0 . If this value is less than or equal to the significance level ($\alpha = 0.05$), H_0 is rejected; if it is greater than the significance level, H_0 is not rejected (Appendix Tab. 5 to 20).

2.5 Diurnal variability of precipitation

For this analysis, the 10-minute database was aggregated to hourly data. A rainy hour was considered to be the hour that recorded at least the minimum rainfall accumulation obtained in the sensitivity analysis of the rainfall event selection. To understand the diurnal variability of precipitation, accumulated precipitation (PA) and frequency (PF) were used. In this context, for each hour of the day, from 00:00 to 23:00 local solar time (LTS), PA is the accumulated precipitation divided by the number of hours, while PF is the percentage of hours with precipitation relative to the total number of hours (ZHANG et al. 2014, ZHOU et al. 2008). Similar to Section 2.4, La Niña and El Niño phases were analyzed separately.

3 Results

3.1 Rainfall events selection

Minimum inter-event time (MIT) of 90 and 60 minutes were defined for lowland (2 and 22 m asl) and highland (422, 619 and 849 m asl), respectively, regardless of the ENSO phase (Appendix Fig 10). The minimum rainfall accumulation was set at 0.2 mm for all altitudes and in both ENSO phases in order to exclude extremely light rainfall events (Appendix Fig 11), since the events defined only by

the MIT showed very small accumulations, mainly concentrated in a duration of 10 minutes (Appendix Fig. 12 to 17).

In Table 2, during La Niña, no increase in the number of events was observed in the altitude range between 2 and 422 m asl on the windward side. However, total rainfall accumulation showed an increase with altitude. During El Niño, the opposite pattern was observed: the number of events increased with altitude, but the total rainfall accumulation decreased in the altitude range between 422 and 849 m asl on the same side of the island. Fewer events were recorded at 422 m asl than at 849 m asl, but the total rainfall accumulation at 422 m asl was about 1.4 times higher than at 849 m asl.

3.2 Altitudinal differences of event-scale precipitation characteristics

3.2.1 Rainfall events

During La Niña, a clear difference in event-scale precipitation characteristics (ESPC) were observed at different altitudes, especially on the windward side. The events with the lowest and highest intensities (mean and maximum) and durations were recorded in this site (Fig. 2a, 2b, 2c). The events with the lowest rainfall intensities and the most variable and prolonged durations were recorded at the highest point of the island, at 849 m asl, while the events with the highest rainfall intensities occurred at 422 m asl. However, the intensity was not significantly different between 2 and 849 m asl and between 422 and 619 m asl. Furthermore, the event duration at 849 m asl was significantly different from most other altitudes, except at 619 m asl. As for rainfall accumulation, it was relatively higher at 422 m asl (Fig. 2d) but was not significantly different at 619 m asl. In Fig. 2d, mean rainfall event accumulation showed high values at 422 and 619 m asl, while low values were recorded at 849 m asl. However, it is at this altitude that the highest total rainfall accumulation was observed, which more than double that of the other altitudes (Tab. 2).

During El Niño, significant differences were observed in most of the ESPC at 849 m asl (Fig. 3a, 3b, 3c), except for rainfall accumulation, where no significant differences were found with respect to the 22 and 619 m asl (Fig. 3d). Rainfall events with lower intensities (mean and maximum) and longer durations occurred at 849 m asl. Durations at this altitude were significantly different from those at other altitudes. However, no significant differences in duration were

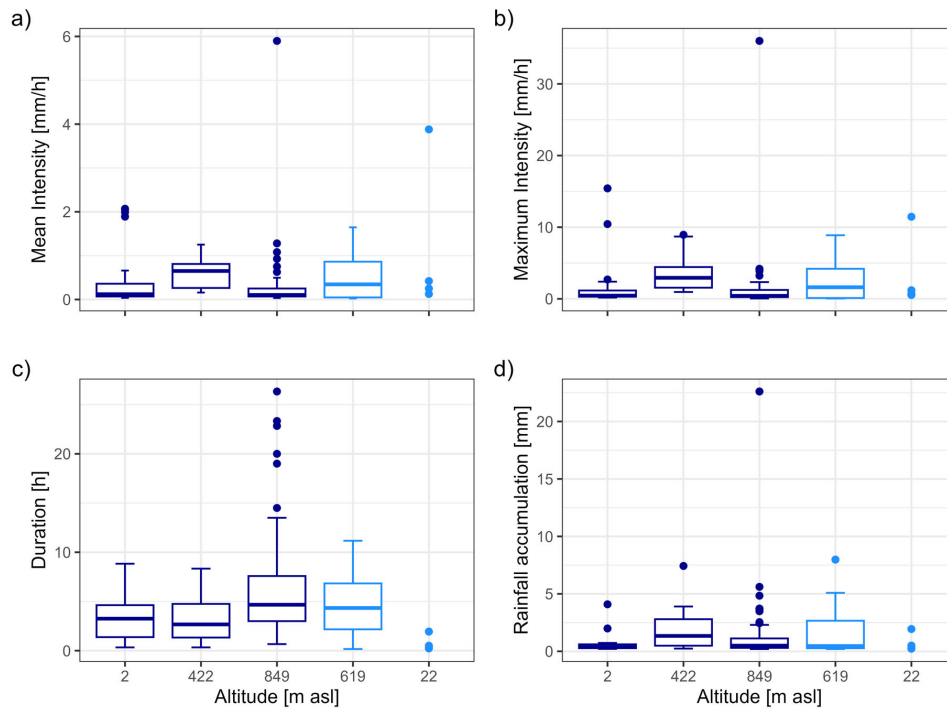


Fig. 2: Boxplots of event-scale precipitation characteristics during La Niña at different altitudes, shown according to the location of altitudes from south to north: a) mean intensity, b) maximum intensity, c) event duration and d) rainfall accumulation. The blue boxplots represent the windward side, while the light blue boxplots represent the leeward side. The horizontal lines within the box represent the median and the interquartile range. The end of the vertical lines represents the lower limit and the upper limit. Each dot represents an outlier, i.e. a characteristic of a rare or extreme event. For the altitude of 22 m asl, a boxplot was not constructed due to the small number of events recorded.

observed among the rest of the altitudes (Fig. 3c). Between 2 and 422 m asl on the windward side and 22 and 619 m asl on the leeward side, a similarity in each of the ESPC were observed. However, the differences between the windward and leeward sides were observed in the outlier, which were higher on the windward side. Rainfall accumulation was similar at most altitudes (Fig. 3d). However, the highest values of total rainfall accumulation were recorded on the windward side, especially at 422 m asl (Tab. 2).

3.2.1 Garúa events

Table 3 shows that during La Niña, the percentage of garúa events ranged from 74% to 97% of the total events (Tab. 2). The highest percentages were observed on the windward side, especially at 849 m asl, where almost 100% of the rainfall events were garúa events. A similar behavior was observed in the percentage of the total rainfall accumulation of these events. On the windward side,

Tab. 2: Number of events and total rainfall accumulation during the two ENSO phases: Rainfall events were defined according to an MIT of 60 min for the highlands and 90 min for the lowlands, a minimum duration of 10 min, and a minimum rainfall accumulation of 0.2 mm. It is shown according to the location of altitudes from south to north, as well as on the windward and leeward sides.

Altitude (m asl)	Side	La Niña		El Niño	
		Rainfall Events	Total Rainfall Accumulation [mm]	Rainfall Events	Total Rainfall Accumulation [mm]
2	Windward	30	18	130	196
422	Windward	19	36	173	610
849	Windward	114	127	235	435
619	Leeward	27	44	69	179
22	Leeward	4	3	39	127

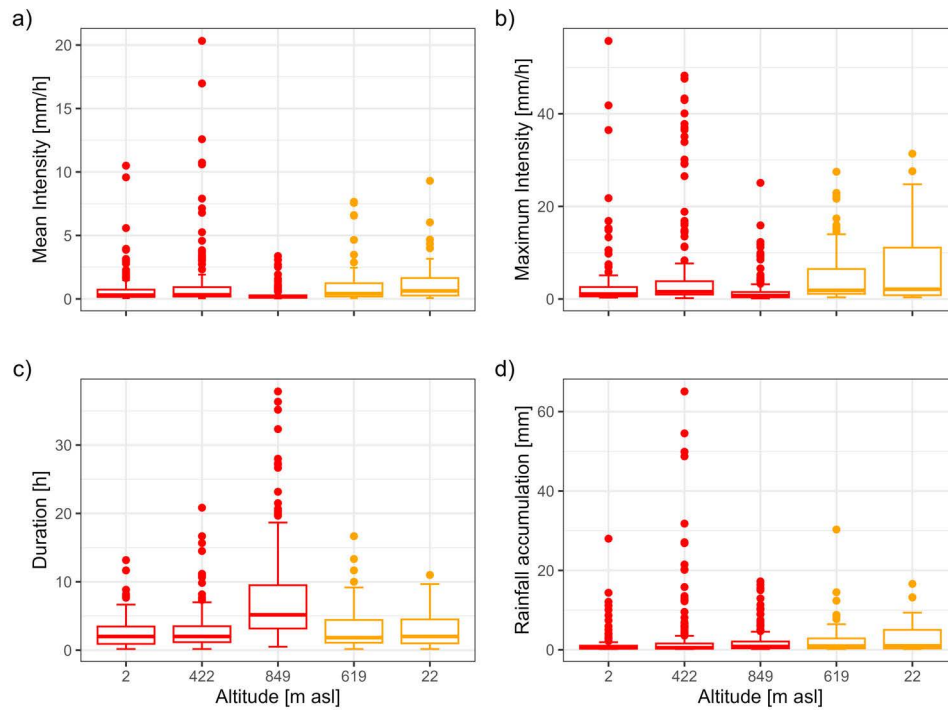


Fig. 3: Boxplots of event-scale precipitation characteristics during El Niño at different altitudes, shown according to the location of altitudes from south to north: a) mean intensity, b) maximum intensity, c) rainfall accumulation and d) duration of the event. The red boxplots represent the windward side, while the orange boxplots represent the leeward side. The horizontal lines within the box represent the median and the interquartile range. The end of the vertical lines represents the lower limit and the upper limit. Each dot represents an outlier, i.e. a characteristic of a rare or extreme event.

this percentage was more than 50%, reaching 80% at 849 m asl, while on the leeward side it was less than 40%.

In general, the behavior of the characteristics of the garúa events were similar to the characteristics of all the rainfall events recorded during La Niña phase. However, the mean intensity, maximum intensity and rainfall accumulation characteristics were lower in the garúa events (Fig. 4). In these events, the highest intensities and rainfall accumulations were recorded at 422 m asl, with significantly different values compared to the other altitudes. Duration was the only characteristic that showed the same range of

variability with respect to the total of rainfall events (Fig. 2), where the longest garúa events occurred at 849 m asl.

During El Niño, the percentage of garúa events showed a similar pattern to that observed during La Niña. In general, more than half of the rainfall events were garúa events (Tab. 3), and at 849 m asl the percentage of these events was almost 100%. However, the contribution of these events to the total rainfall accumulation was less than 40% on the coasts at 2 and 22 m asl, as well as at intermediate altitudes, at 422 and 619 m asl. At 849 m asl, as during La Niña, the largest contribution was recorded.

Tab. 3: Percentage of garúa events and total rainfall accumulation during La Niña and El Niño. It is shown according to the location of altitudes from south to north, as well as on the windward and leeward sides.

Altitude (m asl)	Side	La Niña		El Niño	
		Rainfall Events [%]	Total Rainfall Accumulation [%]	Rainfall Events [%]	Total Rainfall Accumulation [%]
2	Windward	86.6	57.9	80.7	36.7
422	Windward	84.2	67.6	75.1	17.7
849	Windward	97.4	80.3	96.1	85.5
619	Leeward	74.1	37.7	67.6	27
22	Leeward	75	34.2	61.5	17.4

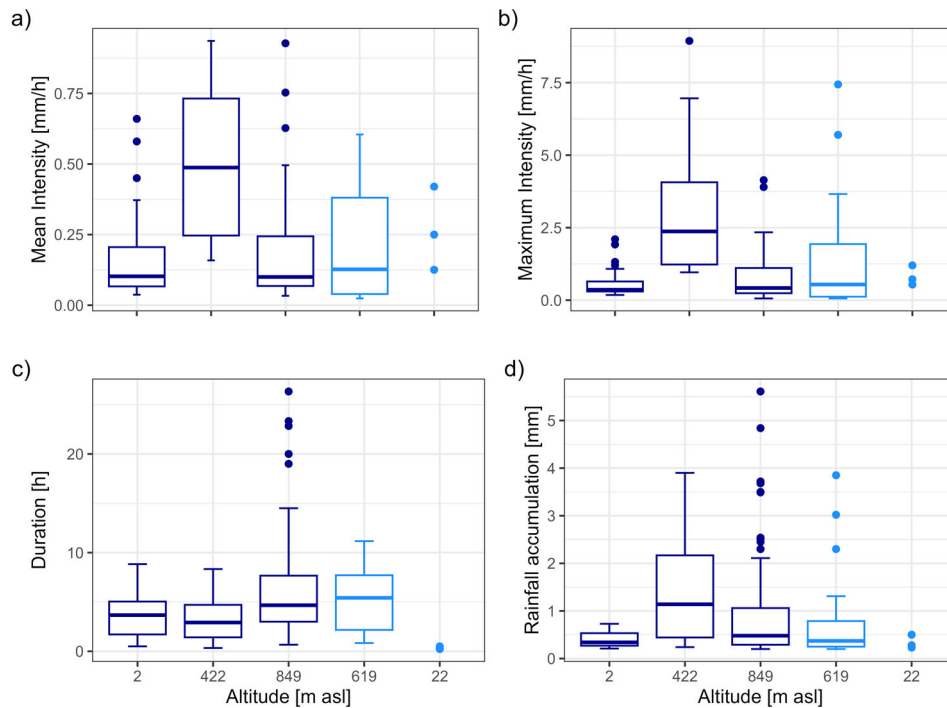


Fig. 4: Boxplots of garúa events characteristic during La Niña at different altitudes, shown according to the location of altitudes from south to north: a) mean intensity, b) maximum intensity, c) event duration and d) rainfall accumulation. The blue boxplots represent the windward side, while the light blue boxplots represent the leeward side. The horizontal lines within the box represent the median and the interquartile range. The end of the vertical lines represents the lower limit and the upper limit. Each dot represents the outliers. For the altitude of 22 m asl, a boxplot was not constructed due to the small number of events recorded.

The behavior of the intensities of the garúa events was similar to that of the total set of rainfall events during El Niño. The highest intensities occurred along the coasts and at intermediate altitudes, while the lowest intensities were observed at 849 m asl (Fig. 5a, 5b). The duration of these events was similar to that of the total set of rainfall events, where the longest events occurred at 849 m asl. At this altitude, all ESPC showed significant differences compared to the other altitudes.

3.3 Diurnal variability of precipitation

During La Niña, the highest accumulated precipitation (PA) on the windward side at 2 and 422 m asl was recorded in the early morning hours of 05:00-06:00 LST (Fig. 6a). However, this was not reflected in the precipitation frequency (PF), which was generally low, especially at times when the PA was high (Fig. 6b). At 849 m asl a maximum PA was recorded at noon at 12:00 LST and a high PF from morning at 06:00 LST to evening at 18:00 LST. On the leeward side, at 619 m asl, continuous rain was recorded from

morning to afternoon, with a high PF at 11:00 – 15:00 LST. At 22 m asl, rainfall was almost zero, with only a few hours of rain in the late afternoon, and its PF was the lowest (Fig. 6).

During El Niño, at 849 m asl, no variability was observed during the diurnal cycle in terms of PA, but a higher PF was observed between morning and noon (Fig. 7). At 2 m asl, although there were certain hours with precipitation peaks, the frequencies were the lowest. Meanwhile, at 422 m asl, the greatest variability in precipitation occurred at 1100-1800 LST, with high frequencies at these times (Fig. 7b). On the leeward side, the PA behavior at 22 and 619 m asl was quite similar, which is also reflected in their PF. The high PA values occurred at 2300-0000 LST did not present high PF as they were concentrated at 1000-1600 LST (Fig. 7).

4 Discussion

In the altitudinal analysis during La Niña, it was observed that the least intense events, with lower rainfall accumulations and longer durations, oc-

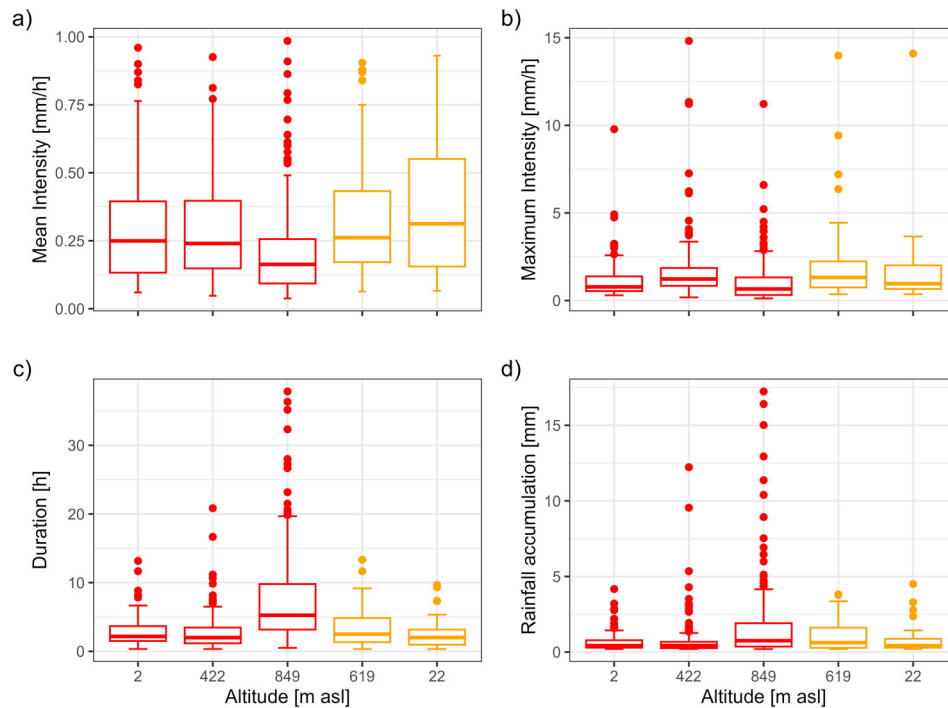


Fig. 5: Boxplots of garúa events characteristic during El Niño at different altitudes, shown according to the location of altitudes from south to north: a) mean intensity, b) maximum intensity, c) event duration and d) rainfall accumulation. The blue boxplots represent the windward side, while the light blue boxplots represent the leeward side. The horizontal lines within the box represent the median and the interquartile range. The end of the vertical lines represents the lower limit and the upper limit. Each dot represents the outliers.

curred at 849 m asl, in the highest peak of the island. The concentration of low intensity values at this altitude may be related to the trade wind inversion (TWI) layer above this altitude, which varies between 900 and 1100 m asl depending on the season (ZANDER et al. 2023). During the cool season, low SST and strengthening trade winds intensify the for-

mation of the TWI layer (TRUEMAN & D'OZOUVILLE 2010). This layer can be further strengthened during La Niña phase, when SST anomalies are negative (WANG et al. 2017). The persistence of this layer prevents moist air from rising, leading to frequent fog and stratus cloud formation over Santa Cruz Island (CONROY et al. 2008, MARTIN et al. 2018, SACHS &

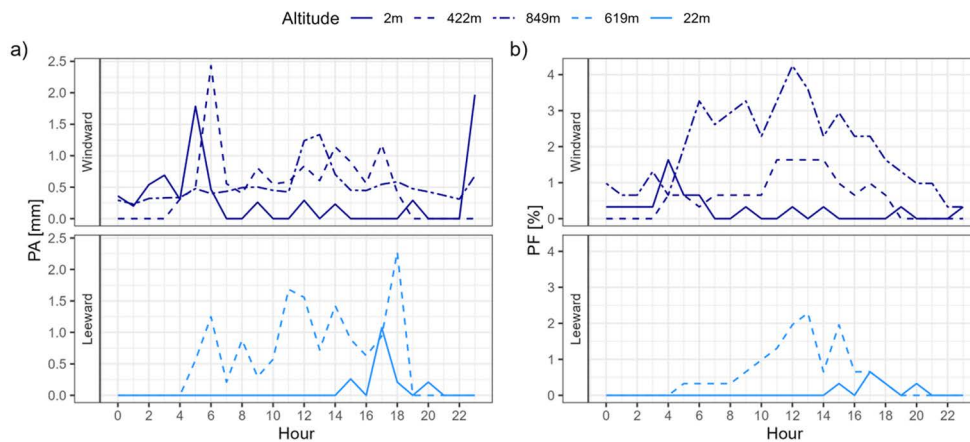


Fig. 6: Diurnal variability of precipitation during La Niña in terms of a) accumulated precipitation (PA) and b) precipitation frequency (PF)

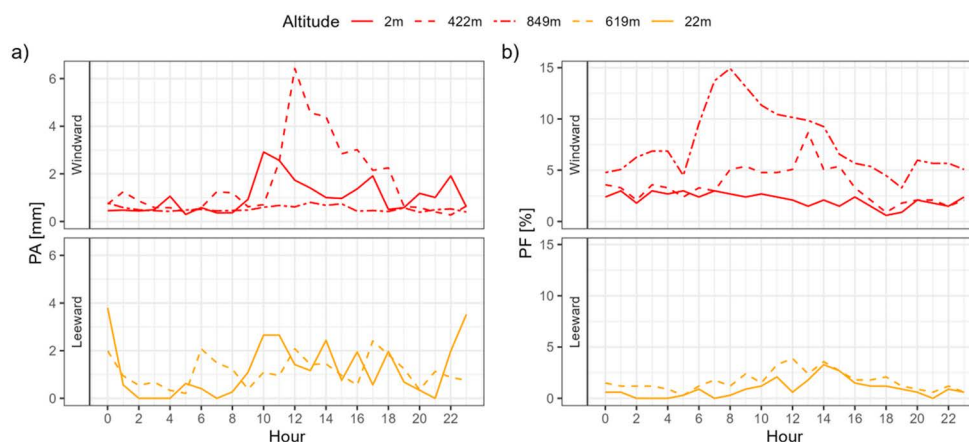


Fig. 7: Diurnal variability of precipitation during El Niño in terms of a) accumulated precipitation (PA) and b) precipitation frequency (PF)

LADD 2010). As a result, at 849 m asl, almost 100% of the events recorded were garúa events, which contributed 80.3% of the total rainfall accumulation at this altitude. These events are consistent with the results of an isotopic study of daily precipitation events on the same island. In this study, most of the events that occurred during La Niña were classified as drizzle or light rain of local origin, known as ‘garúa’ (MARTIN et al. 2018). The lower number of events at 22 m asl can be attributed to a very low cloud formation on the leeward side of the island, at lower altitudes (ZANDER et al. 2023). However, a large total rainfall accumulation was recorded at 619 m asl on the leeward side, second only to that at 849 m asl. This suggests that the stratiform clouds generated on the windward side extend to the leeward side at 619 m asl, which is relatively close to 849 m asl (Fig. 1), leading to precipitation formation.

The diurnal variability of precipitation is closely linked to the temporal evolution of low-level convergences and wind vectors, as well as cloud migration modulated by the land-sea breeze system (HASSIM et al. 2016, MARZUKI et al. 2021). In this context, during La Niña, a different behavior was observed for the windward and leeward sides, where the peak of accumulated precipitation (PA) occurred in the morning and late afternoon, respectively. On the other hand, at the top of the island, this peak occurred at noon. On the windward side, the migration of the PA peaks between 422 and 849 m asl may be attributed to mechanical forcing, where moisture-laden air is forced upward by colliding with the topography. Similarly, this type of behavior may be enhanced by the influence of the sea breeze, which causes warm coastal air to rise and cooler, denser sea air to flow towards the coast. This has been observed in studies such as

(CROSMAN & HOREL 2010, MAPES et al. 2003, QIAN 2008), which show that the diurnal cycle of precipitation tends to be driven by both land-sea breezes and mountain-valley wind systems. The orographic process that generates rainfall events on windward slopes in the Hawaiian Islands are similar to that on Santa Cruz Island. In Hawaii, orographic uplift is enhanced by thermally driven diurnal circulations, such as mountain-valley winds and land-sea breezes, resulting in cooling, cloud formation, and precipitation (CHEN & NASH 1994). On the leeward side, at 619 m asl, the large variability in the diurnal cycle may be influenced by the extent of stratiform clouds that manage to move to this altitude, as well as by the presence of cloud columns, as reported during the cold and dry season (ZANDER et al. 2023), which is enhanced by the influence of La Niña.

In the altitudinal analysis during El Niño, the highest intensities of outliers were recorded at the coasts (2 and 22 m asl) and at intermediate altitudes (422 and 619 m asl). However, event durations did not show significant differences between these altitudes. The ESPC at these altitudes are mainly due to high SST and the weakening of the trade winds, which causes increased evaporation and triggers convective storms (CONROY et al. 2008). The high occurrence of these events is due to the fact that El Niño phase covered the main four months of the warm season, which is intensified by El Niño influence, resulting in even warmer warm seasons (PALTÁN et al. 2021, SNELL & REA 1999). The meteorological conditions during El Niño lead to a weakening of the TWI, which favors the formation of vertical clouds at these altitudes, especially on the leeward side, where there is a higher frequency of clouds in the lower areas (ZANDER et al. 2023). This is consist-

ent with the fact that more than half of the events recorded at all altitudes were garúa events; however, their contribution to the total rainfall accumulation does not exceed 18% on the windward side at 422 m asl and 27% on the leeward side. The weakening of the TWI is not as pronounced at 849 m asl, where low intensity and long duration events are still recorded, associated with the presence of stratiform clouds. At this altitude, it was observed that almost 100% of the total events were garúa events and their contribution to the total rainfall accumulation was 85.5%, a higher percentage than that recorded during La Niña. Fig. 8, shows a summary of how cloud form may be associated with altitudinal differences in ESPC during La Niña and El Niño.

During El Niño, precipitation frequency (PF) showed high variability at 849 m asl, where garúa events were most frequent between 08:00 and 14:00 LST. However, this behavior was not observed on the coasts or in the intermediate windward and leeward altitudes. On the windward side, the highest variability of the accumulated precipitation (PA) was recorded at noon, although the PF was not very high on the coast. On the other hand, on the leeward side, a low variability of PF was observed, with a moderate variability of PA extending from morning to evening. This behavior can be attributed to strong local thermal convection caused by solar heating of the earth's surface during the day (WU et al. 2018). On Lanai Island, at an altitude between 411 and 441 m asl on the leeward side, rainfall maxima were recorded almost daily in the afternoon, generated by convection and a sea breeze front. These phenom-

ena are important sources of moisture in these arid areas (LEOPOLD 1948). In the coastal mountains of Sumatra, where convection occurs over a wide area over the mountainous regions (MARZUKI et al. 2021), with high precipitation intensity prevailing in the afternoon, characterized by convective rain (MORI et al. 2004). Similarly, on Hainan Island, low-level convergence associated with the sea-breeze circulation generates moist convection at midday. During La Niña and El Niño, no large variations in nocturnal precipitation were observed, in contrast to what was recorded on Siberut Island, where there is an increase in humidity during the night, which triggers rainfall (WU et al. 2008).

The high percentage of garúa events at 849 m asl and their significant contribution to the total rainfall accumulation during La Niña and El Niño suggest that, even in the face of these extreme climatic variations, there is a significant input of water that plays a crucial role in water resource management and ecosystem conservation. Therefore, continuous recharge is expected in underground reservoirs, such as the basal and suspended aquifers of the fractured basaltic hydrological systems of Santa Cruz Island, whose recharge height is between 160 and 870 m asl (WARRIER et al. 2012). This will facilitate the distribution of brackish water pumped from aquifers (GUYOT-TÉPHANY et al. 2013), which will be used for most activities except drinking and cooking (REYES et al. 2016). Furthermore, in highland ecosystems, high interception of garúa events by vegetation classified as low-elevation dwarf cloud forest is expected (JÄGER et al. 2009, PRYET et al. 2012). The altitudi-

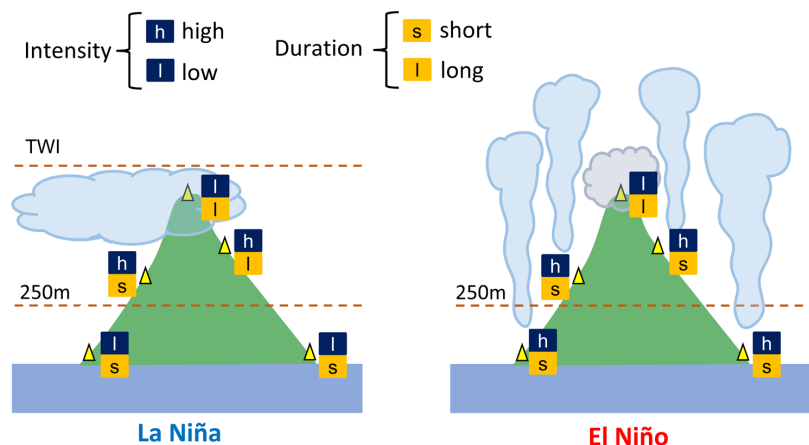


Fig. 8: Summary of the behavior of the intensity and duration of events during La Niña and El Niño phases, and their possible relationship with the dominant cloud types. Convective clouds are shown vertically and stratiform clouds horizontally. The color and letter symbology is detailed at the top of the figure. Leeward side altitudes are shown on the right for each figure.

nal variability of the diurnal cycle of precipitation, as well as the duration and intensity of rainfall events during La Niña and El Niño, could have a significant impact on the region's ecosystems and biodiversity. During El Niño, abundant morning and evening rainfall generally can improve the productivity of terrestrial ecosystems, benefiting land birds such as finches (GRANT & GRANT 1997). However, excessive rainfall has been observed to alter the nesting sites of the American flamingo, reducing its reproductive success (DUEÑAS et al. 2021). It also creates optimal conditions for invasive species that threaten endemic vegetation and fauna (HARRIS & MACDONALD 2007, ONA & DI CARLO 2011). During La Niña, terrestrial ecosystems on the coasts and at intermediate altitudes, especially on the leeward side, would be affected by the generalized decrease in precipitation. This reduction has a negative impact on vegetation and consequently on the availability of food for certain terrestrial species (DUEÑAS et al. 2021).

A comparison between La Niña and El Niño at the same altitude was not conducted in this study due to the different lengths of each phase. La Niña lasted from April 2022 to January 2023, while El Niño lasted from June 2023 to April 2024. In this context, El Niño covered the main months of the rainy season, while La Niña covered only half of the months of this season. Furthermore, it is important to take into account the data gaps that were considered acceptable in this study. On the leeward side, these ranged from 10.9% to 17.2%, a range not significantly influenced by the fact that these regions are considered arid (TRUEMAN & D'OZOUVILLE 2010). However, if these percentages had been recorded on the windward side, where they were less than 7%, they could have introduced a significant bias into the results.

5 Conclusions

This study compares, for the first time, the diurnal cycle and event-scale precipitation characteristics (ESPC) at different altitudes on the windward and leeward sides of Santa Cruz Island in the Galapagos Archipelago during ENSO 2022-2024. To carry out this study, a new network of automatic weather stations was used to record sub-hourly precipitation data. Therefore, the main findings are as follows:

- Altitudinal differences during La Niña were observed in the intensity and duration of rainfall events. At the top of Santa Cruz at 849 m asl, the events were of lower intensity and longer dura-

tion. Furthermore, during El Niño, more convection was observed in coast and at intermediate altitudes, characterized by more intense and shorter duration events. Nevertheless, at 849 m asl, events continued to be of low intensity and long duration, despite the predominance of convection at the lower altitudes.

- During ENSO 2022-2024, more than half of all rainfall events were garúa events. At the top of the island, almost 100% of the events were of this type, contributing 80% and 85% of the total rainfall accumulation during La Niña and El Niño, respectively. However, these percentages varied on the coasts and at intermediate altitudes, ranging from 34% to 67% for La Niña and from 17% to 26% for El Niño.
- The diurnal variability of precipitation, both in amount (PA) and frequency (PF), was influenced by altitude. Maximum variability was observed between morning and afternoon during La Niña and El Niño. However, the PA and PF peaks coincided in the same hour only at 849 m asl during La Niña. At this altitude, regardless of the ENSO phase, the greatest diurnal variability in PF occurred. In contrast, the sides at the windward and leeward coasts (2 and 22 m asl) showed the least variation. Furthermore, the highest PA values were recorded at intermediate altitudes, followed by the coasts, while at 849 m asl the least variability was observed during El Niño, with almost constant PA values.

This study has provided detailed information on rainfall in Santa Cruz, which serves as a basis for a better understanding hydrological processes such as interception, infiltration, runoff, and soil moisture and soil loss. It is also useful for the design of drainage systems to prevent major flooding in urban areas. Furthermore, for the biological sciences, it is essential because during ENSO phases, opportunities are created for terrestrial ecosystems and certain species that benefit from precipitation, while marine ecosystems and other species are vulnerable to changes in SST. The differences in ESPC quantified in this study are of great importance for the research areas mentioned above, especially in the highlands (250 to 849 m asl), which remain humid for most of the year. Future steps should focus on understanding the mechanisms involved in the diurnal cycle of precipitation, as well as the event-scale precipitation characteristics, through a longer study period and the analysis of other meteorological variables. Furthermore, with a larger data set, this study could

be complemented by comparing sub-hourly precipitation during transitions between ENSO phases, including seasonal variations within each phase. It would also be possible to analyse extreme events and their implications for natural resource management and biodiversity conservation by establishing relationships between precipitation and vegetation and faunal processes on the island during periods of drought or heavy rainfall. These studies may be particularly relevant in the Galapagos, given its high climate variability and its role as a sentinel for the effects of climate change.

Acknowledgement

This research was carried out as part of the DARWIN project “Dynamics of Precipitation in Transition: The water source for the Galápagos Archipelago under climate change”, funded by the German Research Foundation (DFG) (BE1780/60-1; SCHE750/18-1) and the Vice-rectorate for Research of Universidad de Cuenca. This publication is contribution number 2730 of the Charles Darwin Foundation for the Galapagos Islands. We thank all members of the DARWIN team for their invaluable support and collaboration during the development of this research. This research was conducted under Galapagos National Park Directorate (GNPD) research permit N° PC-17-25. We are grateful to the Charles Darwin Foundation and Galapagos National Park Directorate (GNPD) for the institutional support. This manuscript is an outcome of the Master of Science Program in Hydrology with a major in Ecohydrology, offered by Universidad de Cuenca.

References

- BALDYSZ Z, NYKIEL G, BARANOWSKI D B, LATOS B, FIGURSKI M (2024) Diurnal variability of atmospheric water vapour, precipitation and cloud top temperature across the global tropics derived from satellite observations and GNSS technique. *Climate Dynamics* 62: 1965–1982. <https://doi.org/10.1007/s00382-023-07005-0>
- BENDIX A, BENDIX J (2006) Heavy rainfall episodes in Ecuador during El Niño events and associated regional atmospheric circulation and SST patterns. *Advances in Geosciences* 6: 43–49. <https://doi.org/10.5194/adgeo-6-43-2006>
- BENDIX J (2000) Precipitation dynamics in Ecuador and northern Peru during the 1991/92 El Niño: A remote sensing perspective. *International Journal of Remote Sensing* 21: 533–548. <https://doi.org/10.1080/014311600210731>
- BRASIL JB, GUERREIRO MS, ANDRADE EMD, DE QUEIROZ PALÁCIO HA, MEDEIROS PHA, RIBEIRO FILHO JC (2022) Minimum rainfall inter-event time to separate rainfall events in a low latitude semi-arid environment. *Sustainability* 14: 1721. <https://doi.org/10.3390/su14031721>
- CARBONE M, TURCO M, BRUNETTI G, PIRO P (2014) Minimum inter-event time to identify independent rainfall events in urban catchment scale. *Advanced Materials Research* 1073-1076: 1630–1633. <https://doi.org/10.4028/www.scientific.net/AMR.1073-1076.1630>
- CHEN W, CHEN C, LI L, XING L, HUANG G, WU C (2015) spatiotemporal analysis of extreme hourly precipitation patterns in Hainan Island, South China. *Water* 7: 2239–2253. <https://doi.org/10.3390/w7052239>
- CHEN Y-L, NASH AJ (1994) Diurnal variation of surface airflow and rainfall frequencies on the island of Hawaii. *Monthly Weather Review* 122. [https://doi.org/10.1175/1520-0493\(1994\)122<0034:dvosaa>2.0.co;2](https://doi.org/10.1175/1520-0493(1994)122<0034:dvosaa>2.0.co;2)
- CHIN RJ, LAI SH, CHANG KB, JAAFAR WZW, OTHMAN F (2016) Relationship between minimum inter-event time and the number of rainfall events in Peninsular Malaysia. *Weather* 71: 213–218. <https://doi.org/10.1002/wea.2766>
- CHU P-S, ZHAO X, RUAN Y, GRUBBS M (2009) Extreme rainfall events in the Hawaiian Islands. *Journal of Applied Meteorology and Climatology* 48: 502–516. <https://doi.org/10.1175/2008JAMC1829.1>
- CONROY JL, OVERPECK JT, COLE JE, SHANAHAN TM, STEINITZ-KANNAN M (2008) Holocene changes in eastern tropical Pacific climate inferred from a Galápagos lake sediment record. *Quaternary Science Reviews* 27: 1166–1180. <https://doi.org/10.1016/j.quascirev.2008.02.015>
- CROSMAN ET, HOREL JD (2010) Sea and lake breezes: A review of numerical studies. *Boundary-Layer Meteorology* 137: 1–29. <https://doi.org/10.1007/s10546-010-9517-9>
- DOMÍNGUEZ CG, PRYET A, GARCÍA VERA M, GONZALEZ A, CHAUMONT C, TOURNEBIZE J, VILLACIS M, D'OZOUVILLE N, VIOLETTE S (2016) Comparison of deep percolation rates below contrasting land covers with a joint canopy and soil model. *Journal of Hydrology* 532: 65–79. <https://doi.org/10.1016/j.jhydrol.2015.11.022>
- DUEÑAS A, JIMÉNEZ-UZCÁTEGUI G, BOSKER T (2021) The effects of climate change on wildlife biodiversity of the galapagos islands. *Climate Change Ecology* 2: 100026. <https://doi.org/10.1016/j.ecochg.2021.100026>
- DUNKERLEY D (2008) Rain event properties in nature and in rainfall simulation experiments: A comparative review with recommendations for increasingly systematic study and reporting. *Hydrological Processes* 22: 4415–4435. <https://doi.org/10.1002/hyp.7045>
- FIENER P, WILKEN F, AUERSWALD K (2019) Filling the gap between plot and landscape scale – eight years of soil erosion monitoring in 14 adjacent watersheds under

- soil conservation at Scheyern, Southern Germany. *Advances in Geosciences* 48: 31–48. <https://doi.org/10.5194/adgeo-48-31-2019>
- GAÁL L, MOLNAR P, SZOLGAY J (2014) Selection of intense rainfall events based on intensity thresholds and lightning data in Switzerland. *Hydrology and Earth System Sciences* 18: 1561–1573. <https://doi.org/10.5194/hess-18-1561-2014>
- GRANT BR, GRANT PR (1997) Evolution of Darwin's finches caused by a rare climatic event. *Proceedings of the Royal Society of London. Series B: Biological Sciences* 251: 111–117. <https://doi.org/10.1098/rspb.1993.0016>
- GRANT PR (1984) Extraordinary rainfall during the El Niño event of 1982–83. *Noticias de Galapagos* 39: 10–11. https://www.darwinfoundation.org/en/documents/292/NG_39_1984.pdf
- GRANT PR, BOAG P T (1980) Rainfall on the Galápagos and the demography of Darwin's Finches. *The Auk* 97: 227–244. <https://doi.org/10.1093/auk/97.2.227>
- GUYOT-TÉPHYANY J, GRENIER C, ORELLANA D (2013) Perceptions, uses and management of water in Galapagos. *Galapagos Report 2011-2012*. Puerto Ayora, Galapago.
- HAMANN O (1979) On climatic conditions, vegetation types, and leaf size in the Galapagos Islands. *Biotropica* 11: 101. <https://doi.org/10.2307/2387785>
- HARRIS DB, MACDONALD DW (2007) Interference competition between introduced black rats and endemic Galápagos Rice Rats. *Ecology* 88: 2330–2344. <https://doi.org/10.1890/06-1701.1>
- HARTMANN DL (2016) Global physical climatology. Amsterdam.
- HASSIM MEE, LANE TP, GRABOWSKI WW (2016) The diurnal cycle of rainfall over New Guinea in convection-permitting WRF simulations. *Atmospheric Chemistry and Physics* 16: 161–175. <https://doi.org/10.5194/acp-16-161-2016>
- JÄGER H, KOWARIK I, TYE A (2009) Destruction without extinction: Long-term impacts of an invasive tree species on Galápagos highland vegetation. *Journal of Ecology* 97: 1252–1263. <https://doi.org/10.1111/j.1365-2745.2009.01578.x>
- JONAITIS JA, PERRY LB, SOULÉ PT, THAXTON C, ANDRADE-FLORES MF, VARGAS TI, TICONA L (2021) Spatiotemporal patterns of ENSO-precipitation relationships in the tropical Andes of southern Peru and Bolivia. *International Journal of Climatology* 4: 4061–4076. <https://doi.org/10.1002/joc.7058>
- JOO J, LEE J, KIM J, JUN H, JO D (2013) Inter-event time definition setting procedure for urban drainage systems. *Water* 6: 45–58. <https://doi.org/10.3390/w6010045>
- KOLIVRAS KN, COMRIE AC (2007) Regionalization and variability of precipitation in Hawaii. *Physical Geography* 28: 76–96. <https://doi.org/10.2747/0272-3646.28.1.76>
- LEOPOLD L B (1948) Diurnal weather patterns on Oahu and Lanai, Hawaii. *Pacific Science* 2: 81–96.
- LI X, MESHGI A, BABOVIC V (2016) Spatio-temporal variation of wet and dry spell characteristics of tropical precipitation in Singapore and its association with ENSO. *International Journal of Climatology* 36: 4831–4846. <https://doi.org/10.1002/joc.4672>
- LI X-F, BLENKINSOP S, BARBERO R, YU J, LEWIS E, LENDERINK G, GUERREIRO S, CHAN S, LI Y, ALI H, VILLALOBOS HERRERA R, KENDON E, FOWLER HJ (2020) Global distribution of the intensity and frequency of hourly precipitation and their responses to ENSO. *Climate Dynamics* 54: 4823–4839. <https://doi.org/10.1007/s00382-020-05258-7>
- LINSLEY RK, KOHLER MA, PAULHUS JLH (1975) Hydrology for Engineers. McGraw-Hill.
- MAIR A, FARES A (2011) Comparison of rainfall interpolation methods in a mountainous region of a tropical island. *Journal of Hydrologic Engineering* 16: 371–383. [https://doi.org/10.1061/\(ASCE\)HE.1943-5584.0000330](https://doi.org/10.1061/(ASCE)HE.1943-5584.0000330)
- MAPES B E, WARNER TT, XU M (2003) Diurnal patterns of rainfall in Northwestern South America. Part III: Diurnal gravity waves and nocturnal convection offshore. *Monthly Weather Review* 131: 830–844. [https://doi.org/10.1175/1520-0493\(2003\)131%3C0830:DPORIN%3E2.0.CO;2](https://doi.org/10.1175/1520-0493(2003)131%3C0830:DPORIN%3E2.0.CO;2)
- MARTIN NJ, CONROY JL, NOONE D, COBB KM, KONECKY BL, REA S (2018) Seasonal and ENSO Influences on the stable isotopic composition of Galápagos precipitation. *Journal of Geophysical Research: Atmospheres* 123: 261–275. <https://doi.org/10.1002/2017JD027380>
- MARZUKI M, SURYANTI K, YUSNAINI H, TANGANG F, MUHARSYAH R, VONNISA M, DEVIANTO D (2021) Diurnal variation of precipitation from the perspectives of precipitation amount, intensity and duration over Sumatra from rain gauge observations. *International Journal of Climatology* 41: 4386–4397. <https://doi.org/10.1002/joc.7078>
- MINEA G, ILIESCU M, DEDU F (2016) Temporal rainfall properties at events scale in the Curvature Subcarpathians (Romania). *Forum Geografic XV* (Supplement 2): 115–123. <https://doi.org/10.5775/fg.2016.141.s>
- MORI S, JUN-ICHI H, TAUHID Y I, YAMANAKA MD, OKAMOTO N, MURATA F, SAKURAI N, HASHIGUCHI H, SRIBIMAWATI T (2004) Diurnal land–sea rainfall peak migration over Sumatera Island, Indonesian maritime continent, observed by TRMM Satellite and intensive rawinsonde soundings. *Monthly Weather Review* 132: 2021–2039. [https://doi.org/10.1175/1520-0493\(2004\)132%3C2021:DLRPMO%3E2.0.CO;2](https://doi.org/10.1175/1520-0493(2004)132%3C2021:DLRPMO%3E2.0.CO;2)
- NIX SJ (1994) Urban stormwater modeling and simulation. Boca Raton.
- NOJUMUDDIN NS, YUSOF F, YUSOP Z (2018) Determination of minimum inter-event time for storm characterisation in Johor, Malaysia. *Journal of Flood Risk Management* 11: S687–S669. <https://doi.org/10.1111/jfr3.12242>

- OÑA IL, DI CARLO G, WWF and CONSERVATION INTERNATIONAL (eds) (2011) Climate change vulnerability assessment of the Galapagos Islands. <https://www.cbd.int/doc/lifeweb/Ecuador/images/ClimateChangeReport.pdf>
- ORELLANA-ALVEAR J, CÉLLERI R, ROLLENBECK R, BENDIX J (2017) Analysis of rain types and their Z–R relationships at different locations in the High Andes of Southern Ecuador. *Journal of Applied Meteorology and Climatology* 56: 3065–3080. <https://doi.org/10.1175/JAMC-D-17-0009.1>
- PADRÓN RS, WILCOX BP, CRESPO P, CÉLLERI R (2015) Rainfall in the Andean Páramo: New insights from high-resolution monitoring in Southern Ecuador. *Journal of Hydrometeorology* 16: 985–996. <https://doi.org/10.1175/JHM-D-14-0135.1>
- PALTÁN HA, BENITEZ FL, ROSERO P, ESCOBAR-CAMACHO D, CUESTA F, MENA CF (2021) Climate and sea surface trends in the Galapagos Islands. *Scientific Reports* 11: 14465. <https://doi.org/10.1038/s41598-021-93870-w>
- PRIAMBODO S, SUHARDJONO, MONTARCIH L, SUHARTANTO E (2019) Hourly rainfall distribution patterns in Java island. *MATEC Web of Conferences* 276: 04012. <https://doi.org/10.1051/mateconf/201927604012>
- PRYET A, DOMÍNGUEZ C, TOMAI PF, CHAUMONT C, D'OZOUVILLE N, VILLACÍS M, VIOLETTE S (2012) Quantification of cloud water interception along the windward slope of Santa Cruz Island, Galapagos (Ecuador). *Agricultural and Forest Meteorology* 161: 94–106. <https://doi.org/10.1016/j.agrformet.2012.03.018>
- QIAN J-H (2008) Why precipitation is mostly concentrated over islands in the maritime continent. *Journal of the Atmospheric Sciences* 65: 1428–1441. <https://doi.org/10.1175/2007JAS2422.1>
- RÉCHOU A, FLORES O, JUMAUX G, DUFLLOT V, BOUSQUET O, POUPEVILLE C, BONNARDOT F (2019) Spatio-temporal variability of rainfall in a high tropical island: Patterns and large-scale drivers in Réunion Island. *Quarterly Journal of the Royal Meteorological Society* 145: 893–909. <https://doi.org/10.1002/qj.3485>
- REYES MF, TRIFUNOVIĆ N, SHARMA S, KENNEDY M (2016) Data assessment for water demand and supply balance on the island of Santa Cruz (Galápagos Islands). *Desalination and Water Treatment* 57: 21335–21349. <https://doi.org/10.1080/19443994.2015.1119756>
- RHOADES O, BRANDT M, WITMAN J (2024) Extinction debt of Galápagos foundational coral associates: ENSO-related cold-water bleaching triggers community biodiversity loss and turnover. *Authorea Preprints*. <https://doi.org/10.22541/au.170663490.09205607/v1>
- SACHS JP, LADD SN (2010) Climate and oceanography of the Galapagos in the 21st century: Expected changes and research needs. *Galapagos Research* 67: 50–54. https://www.darwinfoundation.org/en/documents/387/GR_67_2010.pdf
- SADRAS VO (2003) Influence of size of rainfall events on water-driven processes. I. Water budget of wheat crops in south-eastern Australia. *Australian Journal of Agricultural Research* 54: 341–351. <https://doi.org/10.1071/ar02112>
- SANCHEZ-MORENO JF, MANNAERTS CM, JETTEN V (2014) Influence of topography on rainfall variability in Santiago Island, Cape Verde. *International Journal of Climatology* 34: 1081–1097. <https://doi.org/10.1002/joc.3747>
- SHARMA KK, VERDON-KIDD DC, MAGEE AD (2021) A decision tree approach to identify predictors of extreme rainfall events – A case study for the Fiji Islands. *Weather and Climate Extremes* 34: 100405. <https://doi.org/10.1016/j.wace.2021.100405>
- SMITH RB, SCHAFER P, KIRSHBAUM DJ, REGINA E (2009) Orographic precipitation in the tropics: experiments in Dominica. *Journal of the Atmospheric Sciences* 66: 1698–1716. <https://doi.org/10.1175/2008JAS2920.1>
- SNEEL H, REA S (1999) The 1997–98 El Niño in Galapagos: can 34 years of data estimate 120 years of pattern? *Noticias de Galápagos* 60: 11–20. https://www.darwinfoundation.org/en/documents/318/NG_60_1999.pdf
- SOTTILE G, FRANCIANE A, ADELIO G, NOTO LV (2022) A PCA-based clustering algorithm for the identification of stratiform and convective precipitation at the event scale: An application to the sub-hourly precipitation of Sicily, Italy. *Stochastic Environmental Research and Risk Assessment* 36: 2303–2317. <https://doi.org/10.1007/s00477-021-02028-7>
- TANGANG F, FARZANMANESH R, MIRZAEI A, SUPARI, SALIMUN E, JAMALUDDIN AF, JUNENG L (2017) Characteristics of precipitation extremes in Malaysia associated with El Niño and La Niña events. *International Journal of Climatology* 37: 696–716. <https://doi.org/10.1002/joc.5032>
- TANTELINIAINA MFR, CHEN J, ADYEL TM, ZHAI J (2020) Elevation dependence of the impact of global warming on rainfall variations in a tropical island. *Water* 12: 3582. <https://doi.org/10.3390/w12123582>
- TRUEMAN M, D'OZOUVILLE N (2010) Characterizing the Galapagos terrestrial climate in the face of global climate change. *Galapagos Research* 67: 26–37. https://www.darwinfoundation.org/en/documents/387/GR_67_2010.pdf
- TU A, ZENG J, LIU Z, ZHENG H, XIE S (2023) Effect of minimum inter-event time for rainfall event separation on rainfall properties and rainfall erosivity in a humid area of southern China. *Geoderma* 431: 116332. <https://doi.org/10.1016/j.geoderma.2023.116332>
- URGILÉS G, CÉLLERI R, TRACHTE K, BENDIX J, ORELLANA-ALVEAR J (2021) Clustering of rainfall types using micro rain radar and laser disdrometer observations in the tropical Andes. *Remote Sensing* 13: 991. <https://doi.org/10.3390/rs13050991>
- VARGAS FH, HARRISON S, REA S, MACDONALD DW (2006) Biological effects of El Niño on the Galápagos penguin. *Biological Conservation* 127: 107–114. <https://doi.org/10.1016/j.biocon.2005.08.001>

- WANG C, DESER C, YU J-Y, DiNEZIO P, CLEMENT A (2017) El Niño and Southern Oscillation (ENSO): A review. GLYNN PW, MANZELLO DP, ENOCHS IC (eds) *Coral Reefs of the Eastern Tropical Pacific*: 85–106. Dordrecht. https://doi.org/10.1007/978-94-017-7499-4_4
- WANG W, YIN S, XIE Y, NEARING MA, WANG W, YIN S, XIE Y, NEARING MA (2019) Minimum inter-event times for rainfall in the eastern monsoon region of China. *Transactions of the ASABE* 62: 9–18. <https://doi.org/10.13031/trans.12878>
- WARRIER RB, CASTRO MC, HALL CM (2012) Recharge and source-water insights from the Galapagos Islands using noble gases and stable isotopes. *Water Resources Research* 48: 2011WR010954. <https://doi.org/10.1029/2011WR010954>
- WILCOXON F (1992) Individual comparisons by ranking methods. KOTZ S, JOHNSON NL (eds) *Breakthroughs in statistics: Methodology and distribution*: 196–202. Springer. https://doi.org/10.1007/978-1-4612-4380-9_16. New York.
- WINGFIELD JC, HAU M, BOERSMA PD, ROMERO LM, HILLGARTH N, RAMENOFKY M, WREGE P, SCHEIBLING R, KELLEY JP, WALKER B, WIKELSKI M (2018) Effects of El Niño and La Niña Southern Oscillation events on the adrenocortical responses to stress in birds of the Galapagos Islands. *General and Comparative Endocrinology* 259: 20–33. <https://doi.org/10.1016/j.ygcen.2017.10.015>
- WU P, MORI S, HAMADA J-I, YAMANAKA MD, MATSUMOTO J, KIMURA F (2008) Diurnal variation of rainfall and precipitable water over Siberut Island off the western coast of Sumatra Island. *SOLA* 4: 125–128. <https://doi.org/10.2151/sola.2008-032>
- WU Y, HUANG A, HUANG D, CHEN F, YANG B, ZHOU Y, FANG D, ZHANG L, WEN L (2018) Diurnal variations of summer precipitation over the regions east to Tibetan Plateau. *Climate Dynamics* 51: 4287–4307. <https://doi.org/10.1007/s00382-017-4042-x>
- ZANDER S, TURINI N, BALLARI D, BAYAS LÓPEZ S D, CELLERI R, DELGADO MALDONADO B, ORELLANA-ALVEAR J, SCHMIDT B, SCHERER D, BENDIX J (2023) The spatio-temporal cloud frequency distribution in the Galapagos Archipelago as seen from MODIS cloud mask data. *Atmosphere* 14: 1225. <https://doi.org/10.3390/atmos14081225>
- ZHANG Z, LEDUC G, SACHS J P (2014) El Niño evolution during the Holocene revealed by a biomarker rain gauge in the Galápagos Islands. *Earth and Planetary Science Letters* 404: 420–434. <https://doi.org/10.1016/j.epsl.2014.07.013>
- ZHOU T, YU R, CHEN H, DAI A, PAN Y (2008) Summer Precipitation Frequency, Intensity, and Diurnal Cycle over China: A Comparison of Satellite Data with Rain Gauge Observations. *Journal of Climate* 21: 3997–4010. <https://doi.org/10.1175/2008JCLI2028.1>
- ZHU L, MENG Z, ZHANG F, MARKOWSKI PM (2017) The influence of sea- and land-breeze circulations on the diurnal variability of precipitation over a tropical island. *Atmospheric Chemistry and Physics* 17: 13213–13232. <https://doi.org/10.5194/acp-2017-332>

Authors

Pablo Tenelanda
 pablo.tenelandap@ucuenca.edu.ec
 Dr. Johanna Orellana-Alvear
 ORCID: 0000-0002-6206-075X
 johanna.orellana@ucuenca.edu.ec
 Prof. Dr. Rolando Celleri
 ORCID: 0000-0002-7683-3768
 rolando.celleri@ucuenca.edu.ec
 University of Cuenca
 Department of Water Resources and Environmental
 Sciences
 Av. Víctor Manuel Albornoz y Puente de los Cerezos
 Cuenca
 Ecuador

Prof. Dr. Jörg Bendix
 ORCID: 0000-0001-6559-2033
 bendix@geo.uni-marburg.de
 Dr. Nazli Turini
 nazli.turini@geo.uni-marburg.de
 University of Marburg
 Department of Geography
 Deutschhausstraße 12
 35032 Marburg
 Germany

Byron Delgado Maldonado
 ORCID: 0000-0002-5250-0213
 byron.delgado@fcdarwin.org.ec
 Charles Darwin Foundation
 Av. Charles Darwin s/n
 Puerto Ayora
 Galápagos
 Ecuador

Appendix

Quality control, percentage of missing values during El Niño-Southern Oscillation (ENSO) 2022-2024 on Santa Cruz Island.

Tab. 4: Percentage of missing values for each altitude during the study period for La Niña and El Niño

AWS name	Alt (m asl)	La Niña [%]	El Niño [%]
Puerto Ayora	2	6.5	1.3
Santa Rosa	422	0	0
Cerro Crocker	849	0	6.6
Minas Rojas	619	4.3	12.8
Militar	22	17.2	10.9

Study period, the ONI index represents the three-month central moving average of sea surface temperature anomalies in the Niño 3.4 region.

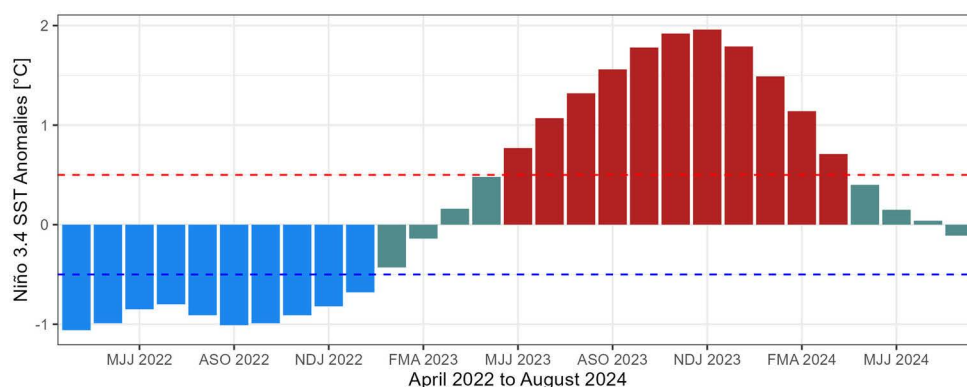


Fig. 9: Evolution of the ONI index from Abril 2022 to August 2024. The blue bars indicate La Niña periods, the red bars correspond to El Niño periods, and the gray bars represent neutral conditions. The blue dashed line indicates an ONI value of -0.5°C , while the red dashed line indicates an ONI value of 0.5°C .

Sensitivity analysis to determine the minimum inter-event time for each altitude during ENSO.

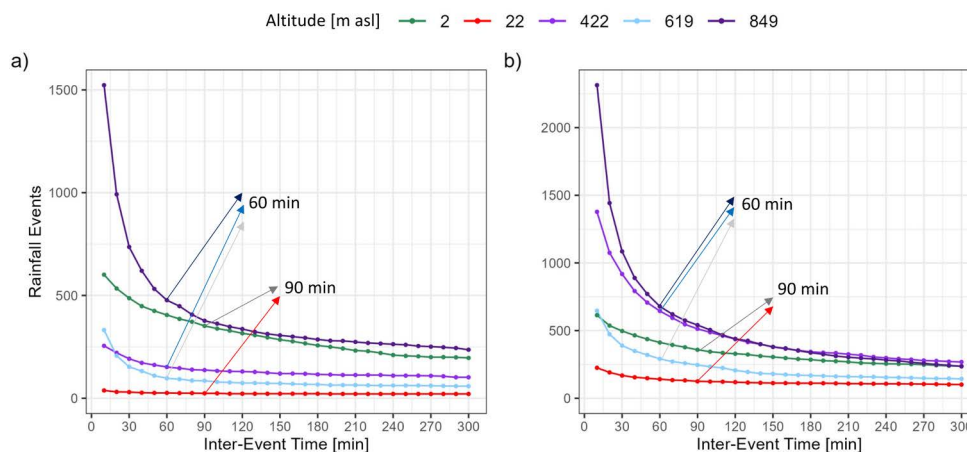


Fig. 10: Sensitivity analysis to determine the minimum inter-event time for each altitude during ENSO: a) La Niña and b) El Niño. Shades of blue show the altitudes located in the highlands, while green and red show the altitudes located in the lowlands. Sensitivity analysis of previously selected events with MIT to determine the minimum rainfall accumulation that an event should have.

Sensitivity analysis of previously selected events with MIT to determine the minimum rainfall accumulation that an event should have.

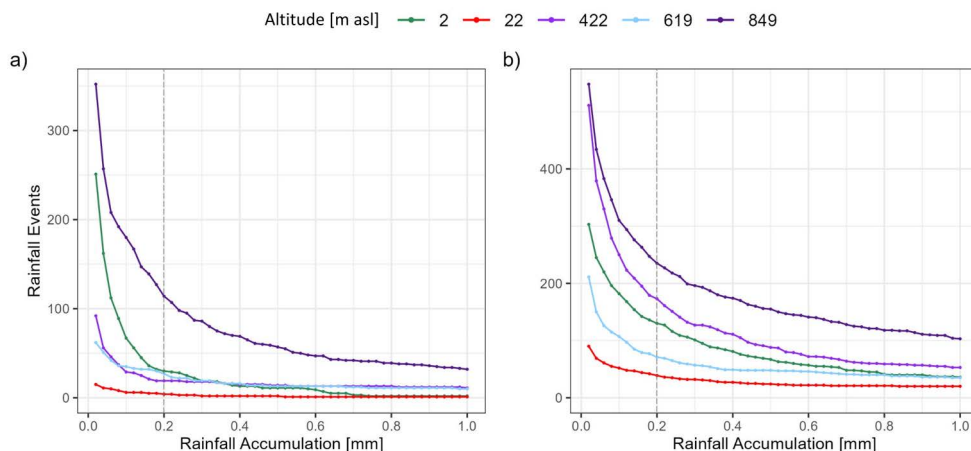


Fig. 11: Sensitivity analysis to determine the minimum rainfall accumulation for each altitude during ENSO: a) La Niña and b) El Niño. Shades of blue show the altitudes located in the highlands, while green and red show the altitudes located in the lowlands. Distribution of precipitation events after selection with a given minimum inter-event time (MIT). This is shown for each elevation during a) La Niña and b) El Niño.

Distribution of precipitation events after selection with a given minimum inter-event time (MIT). This is shown for each elevation during a) La Niña and b) El Niño

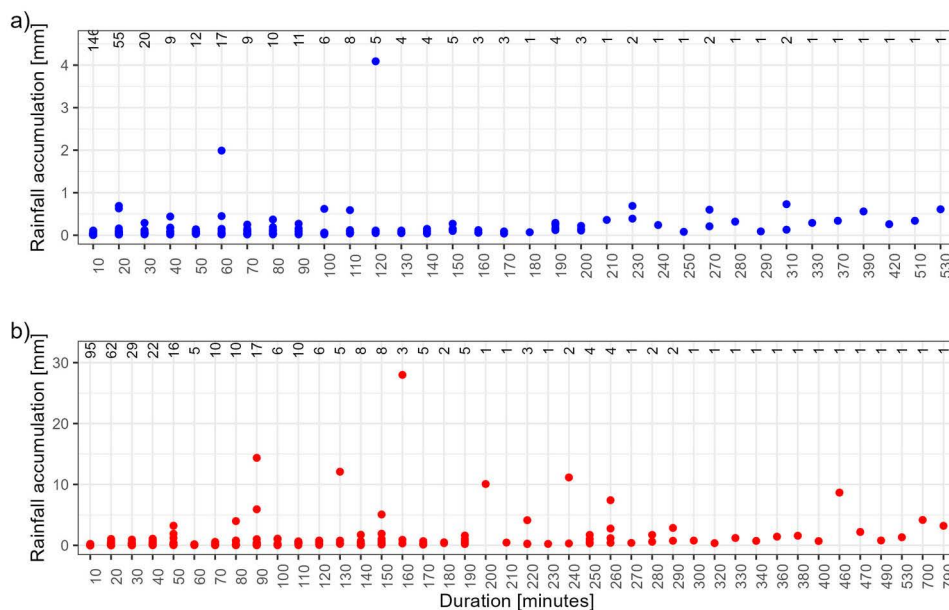


Fig. 12: Rain events selected with a 90-min MIT in Puerto Ayora station at 2 m asl

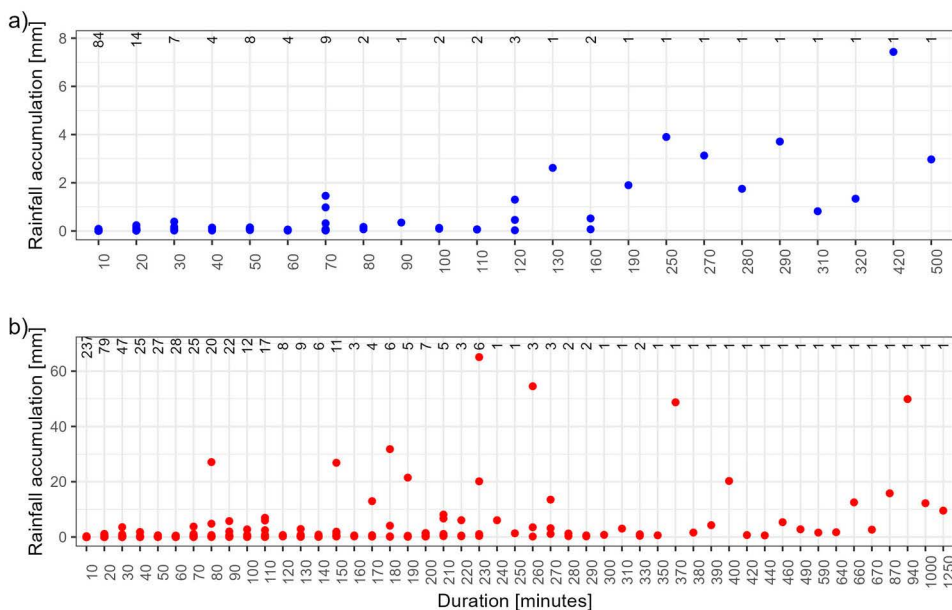


Fig. 13: Rain events selected with a 60-min MIT in Santa Rosa station at 422 m asl

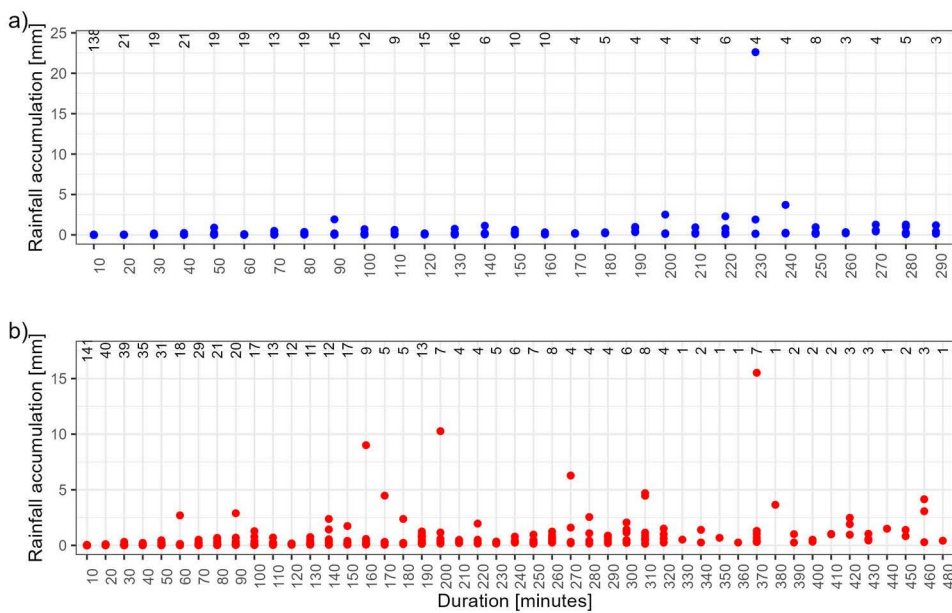


Fig. 14: Rain events selected with a 60-min MIT in Cerro Crocker station at 489 m asl. Durations less than or equal to 290 min and 480 min during La Niña and El Niño, respectively.

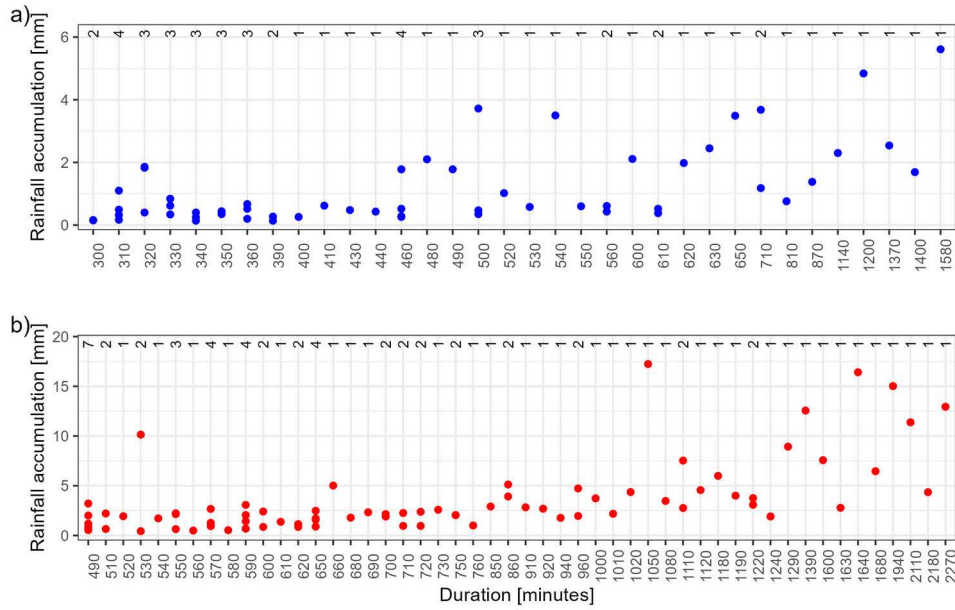


Fig. 15: Rain events selected with a 60-min MIT in Cerro Crocker station at 849 m asl. Durations greater than or equal to 300 min and 490 min during La Niña and El Niño, respectively.

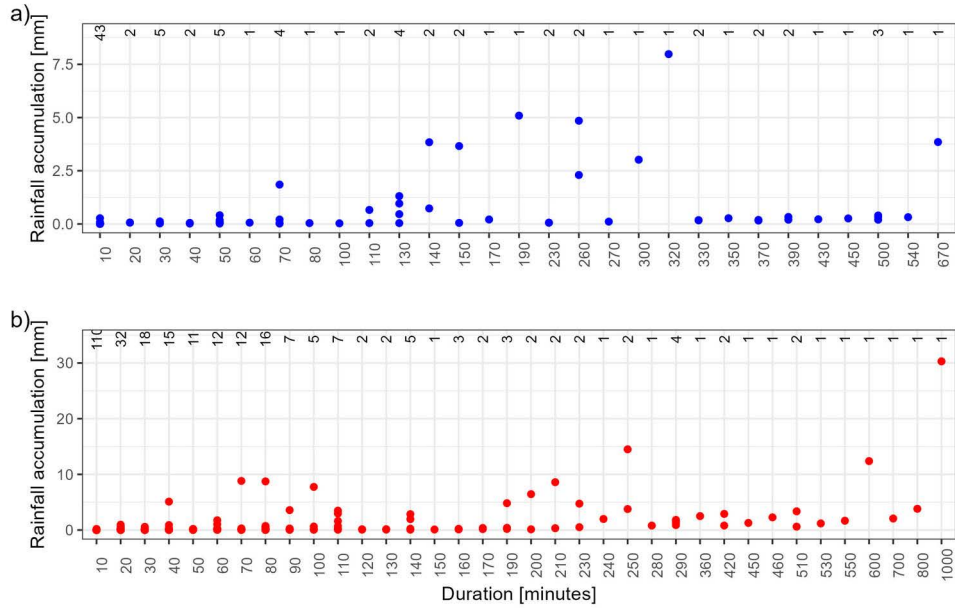


Fig. 16: Rain events selected with a 60-min MIT in Minas Rojas station at 619 m asl

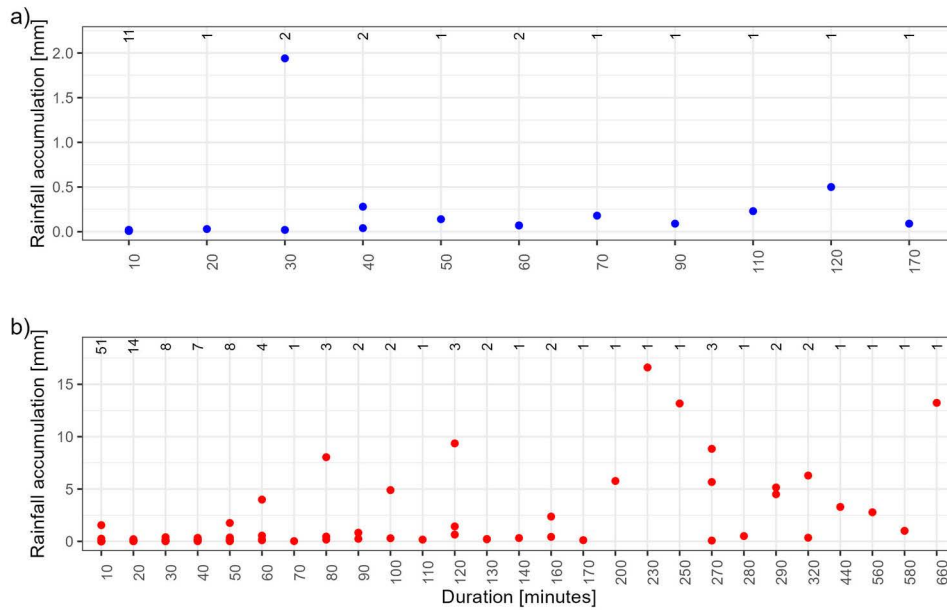


Fig. 17: Rain events selected with a 90-min MIT in Puerto Militar station at 22 m asl

Mann-Whitney U test during El Niña phase for all rainfall events. The p-values obtained when comparing the same ESPC between different altitudes are shown in the tables. At 22 m asl, this test is not reliable due to the insufficient number of events recorded, which was less than four.

Tab. 5: Comparison of mean intensity between different altitudes, values with asterisks have p-values < 0.05

	2 m	422 m	849 m	619 m	22 m
2 m		1E-03*	0.45	0.77	0.14
422 m	1E-03*		1E-07*	0.18	0.61
849 m	0.45	1E-07*		0.12	0.04*
619 m	0.77	0.18	0.12		0.59
22 m	0.14	0.61	0.04*	0.59	

Tab. 7: Comparison of duration between different altitudes, values with asterisks have p-values < 0.05

	2 m	422 m	849 m	619 m	22 m
2 m		0.98	1E-03*	0.17	0.09
422 m	0.98		3E-03*	0.13	0.09
849 m	1E-03*	3E-03*		0.15	1E-03*
619 m	0.17	0.13	0.15		0.01*
22 m	0.09	0.09	1E-03*	0.01*	

Tab. 6: Comparison of maximum intensity between different altitudes, values with asterisks have p-values < 0.05

	2 m	422 m	849 m	619 m	22 m
2 m		2E-05*	0.38	0.50	0.13
422 m	2E-05*		2E-08*	0.051	0.24
849 m	0.38	2E-08*		0.15	0.12
619 m	0.50	0.051	0.15		0.75
22 m	0.13	0.24	0.12	0.75	

Tab. 8: Comparison of rainfall accumulation between different altitudes, values with asterisks have p-values < 0.05

	2 m	422 m	849 m	619 m	22 m
2 m		5E-04*	0.12	0.22	0.89
422 m	5E-04*		5E-03*	0.17	0.14
849 m	0.12	5E-03*		0.61	0.62
619 m	0.22	0.17	0.61		0.66
22 m	0.89	0.14	0.62	0.66	

Mann-Whitney U test during El Niño phase for all rainfall events. The p-values obtained when comparing the same ESPC between different altitudes are shown in the tables.

Tab. 9: Comparison of mean intensity between different altitudes, values with asterisks have p-values < 0.05

	2 m	422 m	849 m	619 m	22 m
2 m		0.37	3E-10*	0.06	0.01*
422 m	0.37		2E-14*	0.25	0.045*
849 m	3E-10*	2E-14*		3E-11*	3E-09*
619 m	0.06	0.25	3E-11*		0.33
22 m	0.01*	0.045*	3E-09*	0.33	

Tab. 10: Comparison of maximum intensity between different altitudes, values with asterisks have p-values < 0.05

	2 m	422 m	849 m	619 m	22 m
2 m		3E-04*	1E-05*	6E-04*	1E-03*
422 m	3E-04*		2E-15*	0.34	0.30
849 m	1E-05*	2E-15*		9E-11*	1E-07*
619 m	6E-04*	0.34	9E-11*		0.54
22 m	1E-03*	0.30	1E-07*	0.54	

Tab. 11: Comparison of duration between different altitudes, values with asterisks have p-values < 0.05

	2 m	422 m	849 m	619 m	22 m
2 m		0.87	1E-22*	0.38	0.59
422 m	0.87		1E-24*	0.44	0.72
849 m	1E-22*	1E-24*		3E-10*	6E-08*
619 m	0.38	0.44	3E-10*		0.82
22 m	0.59	0.72	6E-08*	0.82	

Tab. 12: Comparison of rainfall accumulation between different altitudes, values with asterisks have p-values < 0.05

	2 m	422 m	849 m	619 m	22 m
2 m		0.67	2E-03*	0.01*	0.03*
422 m	0.67		0.02*	0.05	0.11
849 m	2E-03*	0.02*		0.50	0.31
619 m	0.01*	0.05	0.50		0.60
22 m	0.03*	0.11	0.31	0.60	

Mann-Whitney U test during El Niña phase for garúa events. The p-values obtained when comparing the same ESPC between different altitudes are shown in the tables. At 22 m asl, this test is not reliable due to the insufficient number of events, which was less than three.

Tab. 13: Comparison of mean intensity between different altitudes, values with asterisks have p-values < 0.05

	2 m	422 m	849 m	619 m	22 m
2 m		0.18	4E-05*	0.69	0.86
422 m	0.18		0.21	0.57	0.11
849 m	4E-05*	0.21		1E-03*	1E-06*
619 m	0.69	0.57	1E-03*		0.70
22 m	0.86	0.11	1E-06*	0.70	

Tab. 14: Comparison of maximum intensity between different altitudes, values with asterisks have p-values < 0.05

	2 m	422 m	849 m	619 m	22 m
2 m		0.13	1E-06*	0.77	0.97
422 m	0.13		0.02*	0.81	0.34
849 m	1E-06*	0.02*		3E-03*	1E-07*
619 m	0.77	0.81	3E-03*		0.66
22 m	0.97	0.34	1E-07*	0.66	

Tab. 15: Comparison of duration between different altitudes, values with asterisks have p-values < 0.05

	2 m	422 m	849 m	619 m	22 m
2 m		0.12	0.50	0.14	0.01*
422 m	0.12		0.23	0.02*	7E-03*
849 m	0.50	0.23		0.04*	5E-03*
619 m	0.14	0.02*	0.04*		0.64
22 m	0.01*	7E-03*	5E-03*	0.64	

Tab. 16: Comparison of rainfall accumulation between different altitudes, values with asterisks have p-values < 0.05

	2 m	422 m	849 m	619 m	22 m
2 m		0.49	5E-04*	0.60	0.03*
422 m	0.49		0.04*	0.68	0.23
849 m	5E-04*	0.04*		0.02*	0.02*
619 m	0.60	0.68	0.02*		0.34
22 m	0.03*	0.23	0.02*	0.34	

Mann-Whitney U test during El Niño phase for garúa events. The p-values obtained when comparing the same ESPC between different altitudes are shown in the tables.

Tab. 17: Comparison of mean intensity between different altitudes, values with asterisks have p-values < 0.05

	2 m	422 m	849 m	619 m	22 m
2 m		0.28	0.98	0.36	8E-06*
422 m	0.28		0.23	0.70	1E-03*
849 m	0.98	0.23		0.37	1E-06*
619 m	0.36	0.70	0.37		4E-05*
22 m	8E-06*	1E-03*	1E-06*	4E-05*	

Tab. 18: Comparison of maximum intensity between different altitudes, values with asterisks have p-values < 0.05

	2 m	422 m	849 m	619 m	22 m
2 m		0.08	2E-04*	4E-03*	0.01*
422 m	0.08		0.60	0.55	0.01*
849 m	2E-04*	0.60		0.57	7E-09*
619 m	4E-03*	0.55	0.57		1E-05*
22 m	0.01*	0.01*	7E-09*	1E-05*	

Tab. 19: Comparison of duration between different altitudes, values with asterisks have p-values < 0.05

	2 m	422 m	849 m	619 m	22 m
2 m		0.55	0.61	0.35	1E-17*
422 m	0.55		0.66	0.32	2E-06*
849 m	0.61	0.66		0.20	1E-20*
619 m	0.35	0.32	0.20		1E-06*
22 m	1E-17*	2E-06*	1E-20*	1E-06*	

Tab. 20: Comparison of rainfall accumulation between different altitudes, values with asterisks have p-values < 0.05

	2 m	422 m	849 m	619 m	22 m
2 m		0.99	0.43	0.21	7E-06*
422 m	0.99		0.78	0.52	0.03*
849 m	0.43	0.78		0.08	1E-07*
619 m	0.21	0.52	0.08		0.08
22 m	7E-06*	0.03*	1E-07*	0.08	